

Multi-spectral terahertz sensing: proposal for a coupled-cavity quantum cascade laser based optical feedback interferometer

XIAOQIONG QI,¹ GARY AGNEW,¹ IMAN KUNDU,² THOMAS TAIMRE,³ YAH LENG LIM,¹ KARL BERTLING,¹ PAUL DEAN,² ANDREW GRIER,⁴ ALEXANDER VALAVANIS,² EDMUND H. LINFIELD,² A. GILES DAVIES,² DRAGAN INDJIN,^{2,6} AND ALEKSANDAR D. RAKIĆ^{1,5}

¹*School of Information Technology and Electrical Engineering, The University of Queensland, Brisbane, QLD 4072 Australia* ²*School of Electronic and Electrical Engineering, University of Leeds, Leeds LS2 9JT UK*

³*School of Mathematics and Physics, The University of Queensland, Brisbane, QLD 4072 Australia*

⁴*Seagate Technology, Londonderry BT48 0LY, UK*

⁵*rakic@itee.uq.edu.au*

⁶*d.indjin@leeds.ac.uk*

Abstract: We propose a laser feedback interferometer operating at multiple terahertz (THz) frequency bands by using a pulsed coupled-cavity THz quantum cascade laser (QCL) under optical feedback. A theoretical model that contains multi-mode reduced rate equations and thermal equations is presented, which captures the interplay between electro-optical, thermal, and feedback effects. By using the self-heating effect in both active and passive cavities, self-mixing signal responses at three different THz frequency bands are predicted. A multi-spectral laser feedback interferometry system based on such a coupled-cavity THz QCL will permit ultra-high-speed sensing and spectroscopic applications including material identification.

Published by The Optical Society under the terms of the [Creative Commons Attribution 4.0 License](#). Further distribution of this work must maintain attribution to the author(s) and the published article's title, journal citation, and DOI.

OCIS codes: (110.6795) Terahertz imaging; (120.3180) Interferometry; (140.5965) Semiconductor lasers, quantum cascade.

References and links

1. G. Scalari, C. Walther, M. Fischer, R. Terazzi, H. Beere, D. Ritchie, and J. Faist, "THz and sub-THz quantum cascade lasers," *Laser Photon. Rev.* **3**, 45–66 (2009).
2. C. W. I. Chan, Q. Hu, and J. L. Reno, "Ground state terahertz quantum cascade lasers," *Appl. Phys. Lett.* **101**, 151108 (2012).
3. M. Wienold, B. Röben, X. Lü, G. Rozas, L. Schrottke, K. Biermann, and H. T. Grahn, "Frequency dependence of the maximum operating temperature for quantum-cascade lasers up to 5.4 THz," *Appl. Phys. Lett.* **107**, 202101 (2015).
4. L. H. Li, I. Kundu, P. Dean, E. H. Linfield, and A. G. Davies, "High-power GaAs/AlGaAs quantum cascade lasers with emission in the frequency range 4.7–5.6 THz," in *International Quantum Cascade Lasers School and Workshop* (Cambridge, 2016).
5. R. Köhler, A. Tredicucci, F. Beltram, H. E. Beere, E. H. Linfield, A. G. Davies, D. A. Ritchie, R. C. Iotti, and F. Rossi, "Terahertz semiconductor-heterostructure laser," *Nature* **417**, 156–159 (2002).
6. L. H. Li, L. Chen, J. Zhu, J. Freeman, P. Dean, A. Valavanis, A. G. Davies, and E. H. Linfield, "Terahertz quantum cascade lasers with > 1 W output powers," *Electron. Lett.* **50**, 309–311 (2014).
7. S. Fatholouloumi, E. Dupont, C. Chan, Z. Wasilewski, S. Laframboise, D. Ban, A. Mátyás, C. Jirauschek, Q. Hu, and H. C. Liu, "Terahertz quantum cascade lasers operating up to ~ 200 K with optimized oscillator strength and improved injection tunneling," *Opt. Express* **20**, 3866–3876 (2012).
8. B. L. Moran, A. M. Fosnight, and I. R. Medvedev, "Analytical chemical sensing in the thz spectral range," in "Imaging and Applied Optics Technical Papers," (Optical Society of America, 2012), p. SW1C.2.
9. A. J. Fitzgerald, E. Berry, N. N. Zinovev, G. C. Walker, M. A. Smith, and J. M. Chamberlain, "An introduction to medical imaging with coherent terahertz frequency radiation," *Phys. Med. Biol.* **47**, R67 (2002).
10. P. H. Siegel, "Terahertz technology in biology and medicine," *IEEE Trans. Microwave Theory Tech.* **52**, 2438–2447 (2004).

11. J. Federici and L. Moeller, "Review of terahertz and subterahertz wireless communications," *J. Appl. Phys.* **107**, 111101 (2010).
12. F. Mezzapesa, L. Columbo, M. Brambilla, M. Dabbicco, S. Borri, M. Vitiello, H. Beere, D. Ritchie, and G. Scamarcio, "Intrinsic stability of quantum cascade lasers against optical feedback," *Opt. Express* **21**, 13748–13757 (2013).
13. L. Columbo and M. Brambilla, "Multimode regimes in quantum cascade lasers with optical feedback," *Opt. Express* **22**, 10105–10118 (2014).
14. L. Consolino, A. Taschin, P. Bartolini, S. Bartalini, P. Cancio, A. Tredicucci, H. E. Beere, D. A. Ritchie, R. Torre, M. S. Vitiello, and P. De Natale, "Phase-locking to a free-space terahertz comb for metrological-grade terahertz lasers," *Nat. Commun.* **3**, 1040 (2012).
15. S. Barbieri, M. Ravaro, P. Gellie, G. Santarelli, C. Manquest, C. Sirtori, S. P. Khanna, E. H. Linfield, and A. G. Davies, "Coherent sampling of active mode-locked terahertz quantum cascade lasers and frequency synthesis," *Nat. Photonics* **5**, 306–313 (2011).
16. Y. L. Lim, P. Dean, M. Nikolić, R. Kliese, S. P. Khanna, M. Lachab, A. Valavanis, D. Indjin, Z. Ikonjić, P. Harrison, E. H. Linfield, A. G. Davies, S. J. Wilson, and A. D. Rakić, "Demonstration of a self-mixing displacement sensor based on terahertz quantum cascade lasers," *Appl. Phys. Lett.* **99**, 081108 (2011).
17. F. Mezzapesa, M. Petruzzella, M. Dabbicco, H. Beere, D. Ritchie, M. Vitiello, and G. Scamarcio, "Continuous-wave reflection imaging using optical feedback interferometry in terahertz and mid-infrared quantum cascade lasers," *IEEE Trans. Terahertz Sci. Technol.* **4**, 631–633 (2014).
18. A. D. Rakić, T. Taimre, K. Bertling, Y. L. Lim, P. Dean, D. Indjin, Z. Ikonjić, P. Harrison, A. Valavanis, S. P. Khanna, M. Lachab, S. J. Wilson, E. H. Linfield, and A. G. Davies, "Swept-frequency feedback interferometry using terahertz frequency QCLs: a method for imaging and materials analysis," *Opt. Express* **21**, 22194–22205 (2013).
19. Y. L. Lim, T. Taimre, K. Bertling, P. Dean, D. Indjin, A. Valavanis, S. P. Khanna, M. Lachab, H. Schaidler, T. W. Prow, H. P. Soyer, S. J. Wilson, E. H. Linfield, A. G. Davies, and A. D. Rakić, "High-contrast coherent terahertz imaging of porcine tissue via swept-frequency feedback interferometry," *Biomed. Opt. Express* **5**, 3981–3989 (2014).
20. P. Dean, A. Valavanis, J. Keeley, K. Bertling, Y. L. Lim, R. Alhathloul, A. D. Burnett, L. H. Li, S. P. Khanna, D. Indjin, T. Taimre, A. D. Rakić, E. H. Linfield, and A. G. Davies, "Terahertz imaging using quantum cascade lasers — a review of systems and applications," *J. Phys. D: Appl. Phys.* **47**, 374008 (2014).
21. H. S. Lui, T. Taimre, K. Bertling, Y. L. Lim, P. Dean, S. P. Khanna, M. Lachab, A. Valavanis, D. Indjin, E. H. Linfield, A. G. Davies, and A. D. Rakić, "Terahertz inverse synthetic aperture radar imaging using self-mixing interferometry with a quantum cascade laser," *Opt. Lett.* **39**, 2629–2632 (2014).
22. T. Hagelschuer, N. Rothbart, H. Richter, M. Wienold, L. Schrottke, H. T. Grahn, and H.-W. Hübers, "High-spectral-resolution terahertz imaging with a quantum-cascade laser," *Opt. Express* **24**, 13839–13849 (2016).
23. M. Wienold, T. Hagelschuer, N. Rothbart, L. Schrottke, K. Biermann, H. Grahn, and H.-W. Hübers, "Real-time terahertz imaging through self-mixing in a quantum-cascade laser," *Appl. Phys. Lett.* **109**, 011102 (2016).
24. S. Han, K. Bertling, P. Dean, J. Keeley, A. D. Burnett, Y. L. Lim, S. P. Khanna, A. Valavanis, E. H. Linfield, A. G. Davies, D. Indjin, T. Taimre, and A. D. Rakić, "Laser feedback interferometry as a tool for analysis of granular materials at terahertz frequencies: Towards imaging and identification of plastic explosives," *Sensors* **16**, 352 (2016).
25. T. Hagelschuer, M. Wienold, H. Richter, L. Schrottke, K. Biermann, H. Grahn, and H.-W. Hübers, "Terahertz gas spectroscopy through self-mixing in a quantum-cascade laser," *Appl. Phys. Lett.* **109**, 191101 (2016).
26. T. Taimre, M. Nikolić, K. Bertling, Y. L. Lim, T. Bosch, and A. D. Rakić, "Laser feedback interferometry: a tutorial on the self-mixing effect for coherent sensing," *Adv. Opt. Photon.* **7**, 570–631 (2015).
27. G. Agnew, A. Grier, T. Taimre, Y. L. Lim, K. Bertling, Z. Ikonjić, A. Valavanis, P. Dean, J. Cooper, S. P. Khanna, M. Lachab, E. H. Linfield, A. G. Davies, P. Harrison, D. Indjin, and A. D. Rakić, "Model for a pulsed terahertz quantum cascade laser under optical feedback," *Opt. Express* **24**, 20554–20570 (2016).
28. L. Mahler, R. Köhler, A. Tredicucci, F. Beltram, H. E. Beere, E. H. Linfield, D. A. Ritchie, and A. G. Davies, "Single-mode operation of terahertz quantum cascade lasers with distributed-feedback resonators," in "Conference on Lasers and Electro-Optics" (Optical Society of America, 2004), p. CMR1.
29. O. Demichel, L. Mahler, T. Losco, C. Mauro, R. Green, A. Tredicucci, J. Xu, F. Beltram, H. E. Beere, D. A. Ritchie, and V. Tamösiūnas, "Surface plasmon photonic structures in terahertz quantum cascade lasers," *Opt. Express* **14**, 5335–5345 (2006).
30. T. Taimre, K. Bertling, Y. L. Lim, P. Dean, D. Indjin, and A. D. Rakić, "Methodology for materials analysis using swept-frequency feedback interferometry with terahertz quantum cascade lasers," *Opt. Express* **22**, 18633–18647 (2014).
31. L. Ho, M. Pepper, and P. Taday, "Terahertz spectroscopy: Signatures and fingerprints," *Nat. Photon.* **2**, 541 (2008).
32. G. P. Kniffin, S. Schecklman, J. Chen, S. C. Henry, L. M. Zurk, B. Pejcinovic, and A. I. Timchenko, "Measurement and modeling of terahertz spectral signatures from layered material," *Proc. SPIE* **7687**, 768708 (2010).
33. M. S. Vitiello and A. Tredicucci, "Tunable emission in THz quantum cascade lasers," *IEEE Trans. Terahertz Sci. Technol.* **1**, 76–84 (2011).
34. J. Xu, J. M. Hensley, D. Fenner, R. P. Green, L. Mahler, A. Tredicucci, M. G. Allen, F. Beltram, H. E. Beere, and D. A. Ritchie, "Tunable terahertz quantum cascade lasers with an external cavity," *Appl. Phys. Lett.* **91**, 121104 (2007).
35. A. W. M. Lee, B. S. Williams, S. Kumar, Q. Hu, and J. L. Reno, "Tunable terahertz quantum cascade lasers with external gratings," *Opt. Lett.* **35**, 910–912 (2010).
36. N. Han, A. de Geofroy, D. P. Burghoff, C. W. I. Chan, A. W. M. Lee, J. L. Reno, and Q. Hu, "Broadband

- all-electronically tunable MEMS terahertz quantum cascade lasers,” *Opt. Lett.* **39**, 3480–3483 (2014).
37. D. Turčinková, M. I. Amanti, F. Castellano, M. Beck, and J. Faist, “Continuous tuning of terahertz distributed feedback quantum cascade laser by gas condensation and dielectric deposition,” *Appl. Phys. Lett.* **102**, 181113 (2013).
 38. D. Turčinková, M. I. Amanti, G. Scalari, M. Beck, and J. Faist, “Electrically tunable terahertz quantum cascade lasers based on a two-sections interdigitated distributed feedback cavity,” *Appl. Phys. Lett.* **106**, 131107 (2015).
 39. L. Mahler, A. Tredicucci, F. Beltram, H. E. Beere, and D. A. Ritchie, “Tuning a distributed feedback laser with a coupled microcavity,” *Opt. Express* **18**, 19185–19191 (2010).
 40. F. Castellano, V. Bianchi, L. H. Li, J. Zhu, A. Tredicucci, E. H. Linfield, A. Giles Davies, and M. S. Vitiello, “Tuning a microcavity-coupled terahertz laser,” *Appl. Phys. Lett.* **107**, 261108 (2015).
 41. Q. Qin, B. S. Williams, S. Kumar, J. L. Reno, and Q. Hu, “Tuning a terahertz wire laser,” *Nature Photon.* **3**, 732–737 (2009).
 42. S. P. Khanna, M. Salih, P. Dean, A. G. Davies, and E. H. Linfield, “Electrically tunable terahertz quantum-cascade laser with a heterogeneous active region,” *Appl. Phys. Lett.* **95**, 181101 (2009).
 43. C. Wu, Y. Jin, J. L. Reno, and S. Kumar, “Large static tuning of narrow-beam terahertz plasmonic lasers operating at 78 K,” *APL Photonics* **2**, 026101 (2017).
 44. M. Hempel, B. Röben, L. Schrottke, H.-W. Hübers, and H. T. Grahn, “Fast continuous tuning of terahertz quantum-cascade lasers by rear-facet illumination,” *Appl. Phys. Lett.* **108**, 191106 (2016).
 45. I. Kundu, P. Dean, A. Valavanis, L. Chen, L. H. Li, J. E. Cunningham, E. H. Linfield, and A. G. Davies, “Discrete Vernier tuning in terahertz quantum cascade lasers using coupled cavities,” *Opt. Express* **22**, 16595–16605 (2014).
 46. X. Qi, I. Kundu, G. Agnew, A. Grier, T. Taimre, P. Dean, A. Valavanis, L. H. Li, E. Linfield, A. Davies, D. Indjin, and A. D. Rakić, “Frequency tunability in coupled-cavity terahertz quantum cascade lasers,” in “Conference on Optoelectronic and Microelectronic Materials and Devices” (Sydney, Australia, 2016).
 47. X. Qi, I. Kundu, P. Dean, G. Agnew, T. Taimre, A. Valavanis, A. T. Grier, E. H. Linfield, A. G. Davies, D. Indjin, and A. D. Rakić, “Mode selection and tuning mechanisms in coupled-cavity terahertz quantum cascade lasers,” *IEEE J. Sel. Topics in Quantum Electron.* **23**, 1–12 (2017).
 48. I. Kundu, P. Dean, A. Valavanis, L. Chen, L. H. Li, J. E. Cunningham, E. H. Linfield, and A. G. Davies, “Quasi-continuous frequency tunable terahertz quantum cascade lasers with coupled cavity and integrated photonic lattice,” *Opt. Express* **25**, 486–496 (2017).
 49. I. Kundu, P. Dean, A. Valavanis, L. H. Li, E. H. Linfield, and A. G. Davies, “Electrically-controlled frequency tuning of terahertz quantum cascade lasers over 190 GHz using a coupled cavity with integrated photonic lattice,” in “OTST 2017” (London, UK, 2017) *Accepted*.
 50. G. Agnew, A. Grier, T. Taimre, Y. L. Lim, M. Nikolić, A. Valavanis, J. Cooper, P. Dean, S. P. Khanna, M. Lachab, E. H. Linfield, A. G. Davies, P. Harrison, Z. Ikončić, D. Indjin, and A. D. Rakić, “Efficient prediction of terahertz quantum cascade laser dynamics from steady-state simulations,” *Appl. Phys. Lett.* **106**, 161105 (2015).
 51. G. Agnew, A. Grier, T. Taimre, K. Bertling, Y. L. Lim, Z. Ikončić, P. Dean, A. Valavanis, P. Harrison, D. Indjin, and A. D. Rakić, “Temperature dependent high speed dynamics of terahertz quantum cascade lasers,” *IEEE J. Sel. Topics in Quantum Electron.* **23**, 1200209 (2016).
 52. L. Coldren and T. Koch, “Analysis and design of coupled-cavity lasers-part I: Threshold gain analysis and design guidelines,” *IEEE J. Quantum. Electron.* **20**, 659–670 (1984).
 53. L. A. Coldren, S. W. Corzine, and M. L. Mašanović, *Diode Lasers and Photonic Integrated Circuits* (John Wiley & Sons, 2012).
 54. P. Harrison and A. Valavanis, *Quantum Wells, Wires and Dots: Theoretical and Computational Physics of Semiconductor Nanostructures* (Wiley, 2016), 4th ed.
 55. V. Jovanović, S. Höfling, D. Indjin, N. Vukmirović, Z. Ikončić, P. Harrison, J. Reithmaier, and A. Forchel, “Influence of doping density on electron dynamics in GaAs/AlGaAs quantum cascade lasers,” *J. Appl. Phys.* **99**, 103106 (2006).
 56. C. A. Evans, D. Indjin, Z. Ikončić, P. Harrison, M. S. Vitiello, V. Spagnolo, and G. Scamarcio, “Thermal modeling of terahertz quantum-cascade lasers: comparison of optical waveguides,” *IEEE J. Quantum. Electron.* **44**, 680–685 (2008).
 57. C. A. Evans, V. D. Jovanovic, D. Indjin, Z. Ikončić, and P. Harrison, “Investigation of thermal effects in quantum-cascade lasers,” *IEEE J. Quantum. Electron.* **42**, 859–867 (2006).
 58. D. Indjin, P. Harrison, R. Kelsall, and Z. Ikončić, “Self-consistent scattering model of carrier dynamics in GaAs-AlGaAs terahertz quantum-cascade lasers,” *IEEE Photonics Technology Letters* **15**, 15–17 (2003).
 59. D. Indjin, P. Harrison, R. Kelsall, and Z. Ikončić, “Mechanisms of temperature performance degradation in terahertz quantum-cascade lasers,” *Appl. Phys. Lett.* **82**, 1347–1349 (2003).
 60. M. S. Vitiello, G. Scamarcio, V. Spagnolo, C. Worrall, H. E. Beere, D. A. Ritchie, C. Sirtori, J. Alton, and S. Barbieri, “Subband electronic temperatures and electron-lattice energy relaxation in terahertz quantum cascade lasers with different conduction band offsets,” *Appl. Phys. Lett.* **89**, 131114 (2006).
 61. C. H. Henry, “Theory of the linewidth of semiconductor lasers,” *IEEE J. Quantum Electron.* **18**, 259–264 (1982).
 62. S. Tang, D. Saeedkia, and K. Iniewski, *Advances in Imaging and Sensing* (Taylor & Francis Group, LLC, 2016).
 63. S. Barbieri, J. Alton, H. E. Beere, J. Fowler, E. H. Linfield, and D. A. Ritchie, “2.9 THz quantum cascade lasers operating up to 70 K in continuous wave,” *Appl. Phys. Lett.* **85**, 1674 (2004).
 64. M. S. Vitiello, G. Scamarcio, and V. Spagnolo, “Time-resolved measurement of the local lattice temperature in terahertz quantum cascade lasers,” *Appl. Phys. Lett.* **92**, 101116–101116 (2008).

65. A. Valavanis, P. Dean, Y. L. Lim, R. Alhathlool, M. Nikolić, R. Kliese, S. P. Khanna, D. Indjin, S. J. Wilson, A. D. Rakić, E. H. Linfield, and A. G. Davies, "Self-mixing interferometry with terahertz quantum cascade lasers," *IEEE Sens. J.* **13**, 37–43 (2013).

1. Introduction

Terahertz quantum cascade lasers (THz QCLs) are semiconductor sources capable of emitting far infrared radiation in the frequency range 1.2–5.6 THz [1–4]. Since the first THz QCL demonstration in 2002 [5], rapid development has been witnessed over the last decade, and THz QCLs can now emit output powers > 1 W [6] and operate at temperatures of up to ~ 200 K in pulsed mode [7]. The unique features of THz QCLs make them suitable for many relevant applications in the field of chemical sensing, biological and medical imaging, and free-space communications [8–11]. In contrast to conventional interband diode lasers, the intersubband THz QCLs have small linewidth enhancement factors and high photon-to-carrier lifetime ratios, which results in an absence of relaxation oscillations and enhanced stability in strong optical feedback configurations [12]. Furthermore, the multimode dynamical behavior of THz QCLs with strong optical feedback was investigated in [13], where coherent multimode oscillations were obtained indicating spontaneous phase-locking. In addition, the carrier lifetimes in the THz QCLs are dominated by non-radiative phonon scattering phenomena and are typically a few picoseconds. This ultrafast mechanism and related laser dynamics in THz QCLs were also investigated for applications such as frequency comb generation and time-resolved measurements [14, 15].

Recently, THz QCLs with weak optical feedback have been attracting increasing interest in developing applications in sensing, imaging, and spectroscopy [16, 17]. As a coherent sensing technique, laser feedback interferometry (LFI) in THz QCLs has been successfully applied to THz biomedical imaging, explosives detection, and THz radar imaging [18–25]. An LFI system operates via laser radiation reflected back into the laser cavity from an external object, thus giving rise to the "self-mixing" (SM) effect which is measurable in the electronic and optical behavior of the laser [26]. Furthermore, THz QCLs that operate in pulsed current excitation mode are becoming increasingly important, in efforts to increase the temperatures at which these devices operate. THz LFI systems employing pulsed THz QCLs have been modelled recently [27] and, when compared with systems operating in CW regime, predict superior performance including higher optical gain and lower net electrical power consumption.

All THz LFI systems reported to date have employed single-mode THz QCL sources. The intrinsic frequency tuning range of single-mode QCLs by tuning the injection current and temperature are limited on the order of only 0.05 cm^{-1} and 0.1 cm^{-1} (3 GHz), respectively [28, 29]. In these systems the LFI signal is usually generated through frequency modulation by application of a linear current sweep [18, 30].

A wide range of chemicals and biological tissues has multiple characteristic spectral fingerprints in the THz region [31, 32]. In order to facilitate the identification or discrimination of a material with improved accuracy, probing of its optical properties at frequencies near unique spectral features will require tunable THz laser sources. A number of frequency tuning techniques for THz QCLs have been reported [33–44]. These include using external cavities [33–35], microelectromechanical system (MEMS) actuators [36], gas condensation [37], inter-digitated distributed feedback cavities [38], coupled microcavity devices [39, 40], optomechanically coupled QCLs [41], as well as heterogeneous active region in QCLs [42], silicon-dioxide deposition [43] and facet illumination [44]. Large tuning range (≥ 20 GHz) emission has been achieved by applying external grating, MEMS, gas condensation, coupled microcavity devices, optomechanically coupled QCLs, heterogeneous active region or silicon-dioxide deposition on the QCL chips, but suffer from slow tuning [36, 37, 41], operation difficulties [33–35, 39, 43], or device complexity [42]. For example, the approaches reported in [33–35] require separate mechanical control; the silicon-dioxide deposition based solution [43] realized frequency tuning

by control of the thickness of the deposited dioxide; and the size of the external microcavity in [39] was changed by a piezo stage. A robust continuous tuning of THz QCLs around a few GHz have been demonstrated in [38,44]. However, most of techniques above are not monolithic electrically controlled tunable THz sources that are highly desired for LFI sensing applications.

Coupled-cavity (CC) THz QCLs can provide fast frequency tuning by control of the passive cavity current where localized electrical heating in an optically coupled passive cavity permits selection from, and stepping through, several discrete lasing modes [45,46]. We have investigated the mode selection and tuning mechanisms in CC THz QCL based on the transfer-matrix theory and multi-mode reduced rate equations [47]. The frequency tunability in CC THz QCLs have also been demonstrated through self-heating effect and spectral coverage broadening for different active region designs [45,48,49]. In addition, we have established complete dynamic model for THz QCLs that behaves realistically over a wide range of voltages and temperature [50,51].

In this work we propose a method for broadband interrogation of materials by combining mode hopping with fine (continuous) tuning of the individual lasing modes. The mode hopping provides wideband, and controlled, coverage of the THz spectrum, whereas the continuous frequency tuning enables the generation of the LFI signal within each frequency band. In our model, we proposed a scheme for the generation of LFI signals by continuously tuning the QCL emission frequency within three different THz bands spaced by 28 GHz. The modes in the described system are not active or passive mode-locked.

Herein, by using self heating induced via driving pulses applied to the active and passive cavities, both continuous frequency tuning and discrete mode hopping are obtained to effectively probe the external target at a series of THz frequency bands. In order to identify a particular material, the geometry of the CC THz QCL structure can in principle be accurately designed and fabricated to permit lasing modes which target specific spectral features. High-resolution spectral imaging [22] and molecular spectroscopy [25] based on tuning the frequency of THz QCLs have been achieved. However, the maximum frequency tuning range via control of the driving current or heat sink temperature was limited to 1.5 GHz. The THz LFI system based on a tuneable CC THz QCL allows for spectrally resolved sensing or imaging at wider frequency tuning range. An LFI system operating in pulsed mode and built around such a CC THz QCL will permit ultra-high-speed sensing for material identification, and if augmented by a fast-scanning mirror, effectively real-time THz image formation in a compact system. The model proposed here provides an important tool for both operational condition designs and CC THz QCL performance prediction in LFI sensing applications. Although we used a CC geometry where the active cavity length is comparable with the passive cavity length, this model and analysis is valid for other CC geometries presented in [48,49]. Results from the model indicate the feasibility of delivering unique spectral features of a target at multiple frequency bands and spectrally resolved imaging.

The article is organized as follows. Section 2 describes the multimode reduced rate equation (RRE) model in the presence of optical feedback for a CC THz QCL. This is followed by mode tunability analysis and the dependence on critical parameters in Sec. 3.1. Multi-spectral LFI signal results driven by the self-heating effect are presented in Sec. 3.2. Finally, Sec. 4 presents our conclusions.

2. Multi-mode RRE model with optical feedback

A CC THz QCL is composed of an active cavity and a passive cavity, which are optically coupled but electrically separated by an air gap [see Fig. 1]. Both cavities have separate electrical contacts allowing individual control of cavity lattice temperature, refractive index, and of the gain with changes in the injection current. The active cavity with length L_a is being electrically driven above the lasing threshold, and the passive cavity with length L_p is being operated at current levels either below threshold or well above optical power rollover point [27] to control the dominant mode of the device. This ensures that the passive cavity is not lasing and can be modelled as a linear

equivalent mirror [52]. The schematic system for a CC THz QCL with optical feedback is shown in Fig. 1. A CC THz QCL is driven by an active cavity current I_a and a passive cavity current I_p . The feedback coupling coefficient κ relates to the emission facet and target reflectivities and the reinjection loss ε is defined in [27]. The relationship between the external cavity length L_{ext} and the external cavity round-trip time is $\tau_{\text{ext}} = 2L_{\text{ext}}n_{\text{ext}}/c$, where n_{ext} is the refractive index of the external cavity and c is the speed of light. When a target is probed at a particular frequency, its effect on the beam is through its reflectivity at that frequency, R , and the phase change imparted to the beam at that frequency, θ_R . A collection of pairs (R, θ_R) at several distinct frequencies can serve as a fingerprint for material identification. For the LFI based sensing applications, any physical variable that is under detection can be described by one of the parameters mentioned above. For example, the moving target or changes in surface relief during a raster scan over the object surface can be described by a time varying $L_{\text{ext}}(t)$, a refractive index of a target can be found from the complex reflectivity R . The values of the parameters mentioned above are all given in Table I.

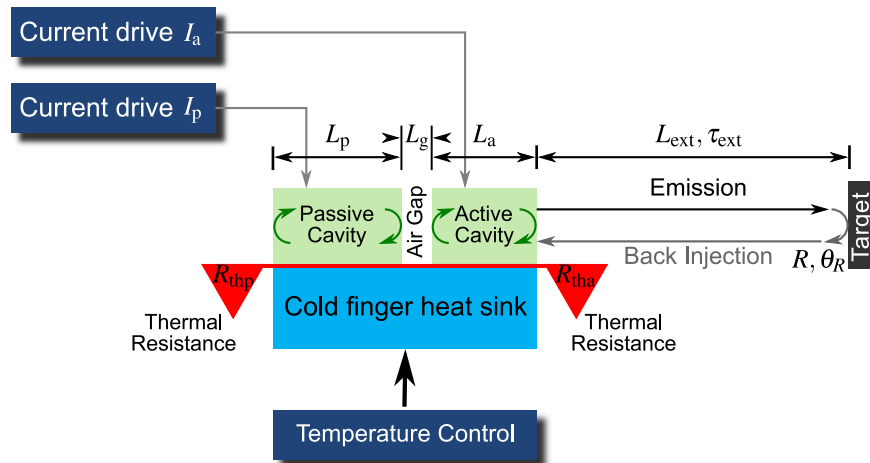


Fig. 1. Optical feedback model for the coupled-cavity THz QCL. The internal cavity has passive cavity of length L_p , air gap of length L_g , and active cavity of length L_a . THz emission is through the facet on the right-hand side of the active cavity and traverses the external cavity of length L_{ext} with refractive index n_{ext} before reflecting back toward the QCL by the target. The power reflectivity and phase change introduced by the target are R and θ_R respectively. The round trip propagation time in the external cavity is τ_{ext} . A portion of the reflected light, dictated by the re-injection loss ε , re-enters the laser and mixes with the field inside the laser cavity, generating the SM signal, which contains information pertaining to the target.

Based on complex scattering transmission matrix theory [53], the air gap and the passive cavity can be represented as an effective complex mirror. As such the CC QCL can be viewed as a single cavity (SC) with an effective complex mirror. The eigenmode frequencies of a CC THz QCL are determined by eigenvalues of the denominator of the transfer function of the device [52]. The frequency-dependent effective complex mirror combined with gain spectrum of the active cavity determines the dominant mode and the side mode suppression ratio (SMSR). In addition, by tuning the amplitude of the passive cavity current, single-mode operation with discrete mode hopping can be achieved by localized electrical heating of the passive cavity [45]. Furthermore, by considering self-heating effect in the active cavity due to the application of active cavity pulses [27], continuous frequency tuning can be obtained as well. Therefore, through the

combination of thermal processes in the coupled cavities and SM effect, we can effectively probe the external target and obtain LFI signal at a series of THz frequency bands. We have earlier presented a dynamical model for single-mode THz QCL in the presence of optical feedback [27]. In this article, we propose a model for CC THz QCL under feedback operating in multi-mode regime. The behavior of a CC THz QCL under optical feedback can be described by the multimode reduced rate equations (RREs) (1)–(4) with the “feedback term” identified by under braces. The time varying lattice temperatures in the active and passive cavities $T_{a,p}(t)$ during the thermal processes can be obtained by solving the thermal Eq. (5). This set of equations reads as follows:

$$\frac{dN_3(t)}{dt} = \frac{\eta_3}{q} I_a(t) - (N_3(t) - N_2(t)) \sum_{m=1}^N G_m S_m(t) - \frac{N_3(t)}{\tau_3}, \quad (1)$$

$$\frac{dN_2(t)}{dt} = \frac{\eta_2}{q} I_a(t) + (N_3(t) - N_2(t)) \sum_{m=1}^N G_m S_m(t) + \frac{N_3(t)}{\tau_{32}} + \frac{N_3(t)}{\tau_{sp}} - \frac{N_2(t)}{\tau_2}, \quad (2)$$

$$\begin{aligned} \frac{dS_m(t)}{dt} = & MG_m(N_3(t) - N_2(t)) S_m(t) - \frac{S_m(t)}{\tau_{p,m}} + M \frac{\beta_{sp}}{\tau_{sp}} N_3(t) \\ & + \underbrace{\frac{2\kappa}{\tau_{in}} (S_m(t) S_m(t - \tau_{ext}))^{\frac{1}{2}} \cos(\omega_{th,m} \tau_{ext} + \varphi_m(t) - \varphi_m(t - \tau_{ext}))}_{\text{Feedback Term}} \\ & m = 1, 2, \dots, N, \end{aligned} \quad (3)$$

$$\begin{aligned} \frac{d\varphi_m(t)}{dt} = & \frac{\alpha}{2} \left(G_m(N_3(t) - N_2(t)) - \frac{1}{\tau_{p,m}} \right) \\ & - \underbrace{\frac{\kappa}{\tau_{in}} \left(\frac{S_m(t - \tau_{ext})}{S_m(t)} \right)^{\frac{1}{2}} \sin(\omega_{th,m} \tau_{ext} + \varphi_m(t) - \varphi_m(t - \tau_{ext}))}_{\text{Feedback Term}} \\ & m = 1, 2, \dots, N, \end{aligned} \quad (4)$$

$$\frac{dT_{a,p}(t)}{dt} = \frac{1}{m_{a,p} c_{a,p}(T)} \left(I_{a,p}(t) V_{a,p}(t) - \frac{(T_{a,p}(t) - T_0(t))}{R_{th,a,p}} \right), \quad (5)$$

where $N_3(t)$ and $N_2(t)$ are the carrier populations in the upper and lower laser levels (ULL/LLL) of the active cavity, respectively, while $S_m(t)$ and $\varphi_m(t)$ represent the photon population and the phase of the electric field in mode m . Equations (3) and (4) each represent N equations for the photon population and the phase for longitudinal eigenmodes. The electron transport parameters ($\eta_3, \eta_2, \tau_3, \tau_2, \tau_{32}$) are obtained from the full self-consistent energy-balance Schrödinger–Poisson scattering transport calculation for the given lasing cavity current I_a described in Refs. [27, 50, 54, 55]. Joule heating due to the change of driving current can markedly affect the active region lattice temperature of THz QCLs [56, 57]. Lattice temperature change would have an influence on electron transport via changes of scattering rates, electron subband lifetimes and electron subbands temperature [58–60]. All these effects were included in electron transport parameters calculation. The photon lifetime $\tau_{p,m}$ is calculated from $\tau_{p,m} = (v_{g,m}(\alpha_a + \alpha_{eff,m}))^{-1}$, where α_a is waveguide loss of the active cavity, $\alpha_{eff,m}$ is the effective mirror loss of the CC THz QCL obtained by transfer matrix method [53], and $v_{g,m}$ is the group velocity for mode m . Once the equations are solved, the emission output power per mode can be calculated by $P_m(t) = \eta_{0,m} \hbar \omega_m S_m(t) / \tau_{p,m}$, where $\eta_{0,m}$ is power output coupling coefficient for mode m [53]. Equation (5) of the thermal model in the active cavity or the passive cavity of a CC THz QCL is a function of the chip mass

of the active or passive cavity $m_{a,p}$, the effective specific heat capacities $c_{a,p}$, the drive currents $I_{a,p}(t)$, and the cold finger temperature T_0 . The meaning of other symbols, together with typical values used in the simulations are summarized in Table 1.

The theoretical model above couples self-heating effect of both active and passive cavities into the multi-mode RREs for the CC THz QCL under optical feedback. Self-heating in the device leads to change in laser frequency: mode tuning and continuous frequency tuning of each dominant mode. We used the former to achieve wide tuning range and the latter to create continuous-wave frequency modulated interferometric signal. However, the effect of optical feedback on the self-heating of the device is neglected since the dominant contributor to heating is electrical power delivered to the device.

3. Results and discussion

3.1. Frequency tunability in free-running CC THz QCLs

A free-running CC THz QCL can be described by multi-mode RREs without the “feedback terms” identified by under braces, given in Eqs. (1)–(5). By setting the left-hand side of the thermal equation for the passive cavity [Eq. (5) for T_p] to zero, the steady state solution is obtained in the form $\Delta T_p = I_p V_p R_{th,p}$ [45]. Changing the current of the passive cavity I_p brings about changes in its lattice temperature, which in turn perturbs the refractive index of the passive cavity [45]. This alters the threshold gain spectrum of the active region through changes to the reflectivity of the effective mirror, and, through the control of the passive cavity current, can result in altering the dominant lasing mode of the device. This current-controlled selection of the lasing frequency (self-adjusted by mode hopping to a mode with the maximum net gain) is the mechanism we propose in order to facilitate the wide-band operation of the device.

The exemplar device selected for modelling is a 150 μm -wide 11.6 μm -thick THz CC QCL with a bound-to-continuum active region based on GaAs/Al_{0.15}Ga_{0.85}As material system, as described in [45, 63]. As shown in Fig. 1, this device contains the active cavity of length $L_a=1.5$ mm, an air gap of $L_g = 13$ μm and a passive cavity of length $L_p=1.582$ mm. The simulation model shows that this structure supports up to seven discrete lasing modes (labelled here M1 through M7) with a significant level of side-mode suppression ratio (SMSR) of above 25 dB, ensuring the single-mode operation at all simulated passive cavity current values. It also demonstrates that by changing the current of the passive cavity one can effectively promote the controlled discrete change in lasing frequency by selecting individual modes in succession. The mechanism of mode tuning of CC THz QCLs through localized Joule heating in the passive cavity was proposed earlier [45].

By selecting the passive cavity current I_p and pulsing the active cavity with the drive current at the above-threshold value [$I_a=0.75$ A, refer to Fig. 3] one achieves the pulsed single-mode operation in modes M4 through M1. The eigenmode frequencies of modes M1 through M7 were calculated at 2.710, 2.738, 2.766, 2.794, 2.822, 2.850, and 2.878 THz. We note that simulated SMSR varies with I_p for each dominant mode and the maximum SMSRs occur when I_p is 0 A, 1.39 A, and 2.05 A for modes M4, M3, and M2, respectively [marked as A, B, and C in Fig.]. The corresponding lattice temperature changes ΔT_p are 0 K, 67.4 K, and 124.8 K, respectively. The output emission spectra of the CC THz QCL for I_p at 0 A, 1.39 A, and 2.05 A are shown in Fig. 2 (b)–2 (d), for which the respective dominant modes M4, M3, and M2 with SMSRs of 25.9 dB, 25.6 dB, and 27.6 dB were obtained.

3.2. Multi-spectral LFI signal generated by thermal processes

A CC THz QCL under optical feedback can be described by the multi-mode RREs with the “feedback terms” identified by under braces, given in Eqs. (1)–(5). Equations (3) and (4), describing the evolution of photon densities and phases for each mode, parallel the assumptions made in the

Table 1. Simulation parameters used in Eqs. (1)–(5).

Symbol	Description	Value / Units
η_3	Injection efficiency into ULL	54 %
η_2	Injection efficiency into LLL	1.65 %
$I_a(t)$	Active cavity drive current	0.75 A
$I_p(t)$	Passive cavity drive current	0 A, 1.39 A, and 2.05 A
L_a	Active cavity length	1.5 mm
L_g	Air gap length	13 μm
L_p	Passive cavity length	1.582 mm
M	Number of periods in active cavity	90
β_{sp}	Spontaneous emission factor	1.627×10^{-4}
τ_3	Total carrier lifetime in ULL	5×10^{-12} s
τ_{32}	Non-radiative relaxation time from ULL to LLL	1.76×10^{-10} s
τ_2	Total carrier lifetime in LLL	2.7×10^{-11} s
τ_{sp}	Spontaneous emission lifetime	5×10^{-10} s
α_a	Waveguide loss of active cavity	9 cm^{-1}
$\alpha_{\text{eff},m}$	Effective mirror loss	Varies
$\omega_{\text{th},m}$	Emission frequency at threshold (no optical feedback)	2.710, 2.738, 2.766, 2.794, 2.822, 2.850, 2.878 THz
G_m	Gain factor for mode m , from mode 1 to 7	1.98, 2.03, 2.07, 2.09, 1.92, 1.76, $1.65 \times 10^4 \text{ s}^{-1}$
τ_{ext}	Round-trip time of the external laser cavity	1.136×10^{-8} s
L_{ext}	External cavity length	1.704 m
n_{ext}	Refractive index of external cavity	1.00
n_{in}	Effective refractive index of active and passive cavity	3.61
κ	Feedback coupling coefficient in external cavity	4.8×10^{-3}
ε	Re-injection loss factor	0.01
R	Reflectivity of external target	0.7
α	Henry's linewidth enhancement factor [61]	-0.1 Refs. [27, 62]
$m_{a,p}$	Effective mass of active and passive cavity	1.39×10^{-8} kg and 1.47×10^{-8} kg
$c_{a,p}$	Effective specific heat capacity of active and passive cavity	$79.6 \text{ J kg}^{-1} \text{ K}^{-1}$
$R_{\text{th},a,p}$	Effective thermal resistance of active and passive cavity	9.082 and 8.612 K W^{-1}
T_0	Sub mount / cold finger temperature	40 K
$T_{a,p}(t)$	Lattice temperature of active region and passive cavity	Varies

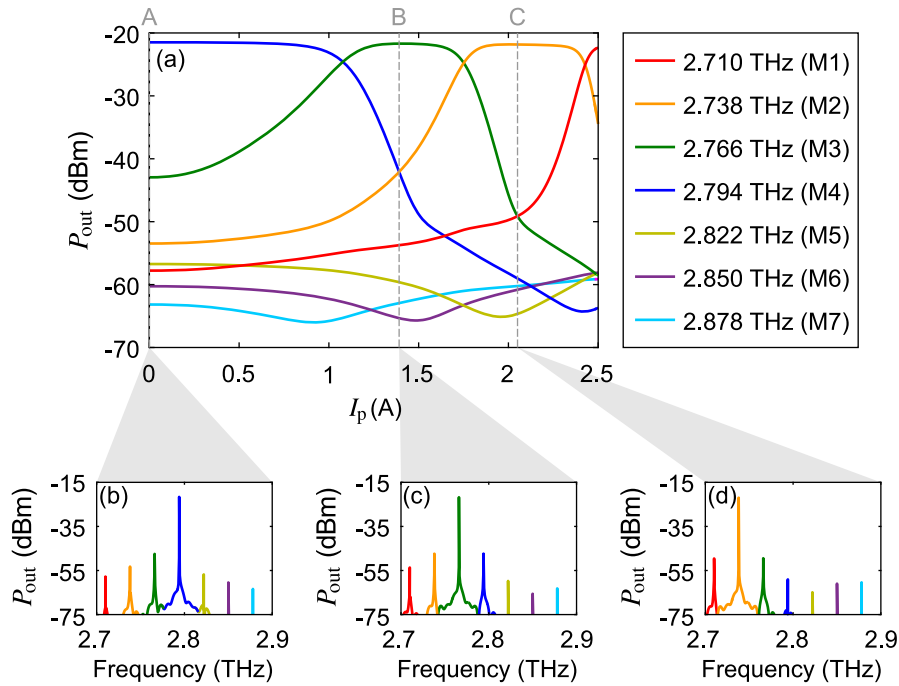


Fig. 2. Mode tunability in a CC THz QCL with $L_a=1.5$ mm, $L_g = 13$ μ m, $L_p=1.582$ mm: (a) Multimode output power P_{out} as a function of the passive current amplitude I_p in the CC THz QCL, and output spectra of the CC THz QCL for three different values of the passive cavity current: (b) $I_p=0$ A, (c) $I_p=1.39$ A, and (d) $I_p=2.05$ A, corresponding to A, B, C, respectively in (a).

Lang and Kobayashi feedback model [26, 27]. From Eq. (5) for T_p and the results of Fig. 2, it is seen that the self-heating effect induced by the driving current I_p is a significant contributor to lattice temperature change in the passive cavity. When the passive cavity is driven by a current pulse, a thermal response follows, with the lattice temperature rising rapidly at first, and then saturating at a steady state value of $T_0 + I_p V_p R_{th,p}$. As noted earlier [64] this numerically obtained thermal response can be approximated by using two exponential functions, or for the sake of simplicity of interpretation, with one effective time constant. The associated equivalent thermal time constant depends on the cold finger temperature T_0 , the electrical power $I_p V_p$, the thermal resistance $R_{th,p}$ of the passive cavity to the cold finger, the mass of the passive cavity chip m_p , and the effective specific heat capacity c_p of the passive cavity material. When the pulse duration in the passive cavity is longer than the thermal time constant, the lattice temperature in the passive cavity saturates, and the dominant mode of the CC THz QCL will change to the mode with maximum net gain. In addition, the self-heating effect can be used in the active cavity to fine-tune the device lasing frequency. As our simulations [refer to Fig. 3] show, the short 2 μ s current pulse applied to the active cavity changes the lattice temperature and results in a continuous red shift of the dominant mode, and not mode hopping.

Combining self-heating effects in both cavities thus allows a selection of the dominant lasing mode (for wide-band coverage) in combination with continuous frequency tuning at each mode. This enables a CC THz QCL to effectively probe the external target at a series of THz frequency bands — resulting in a series of SM signals — so as to interrogate the response of the target under test at multiple frequency bands corresponding to the unique spectral signature of the target.

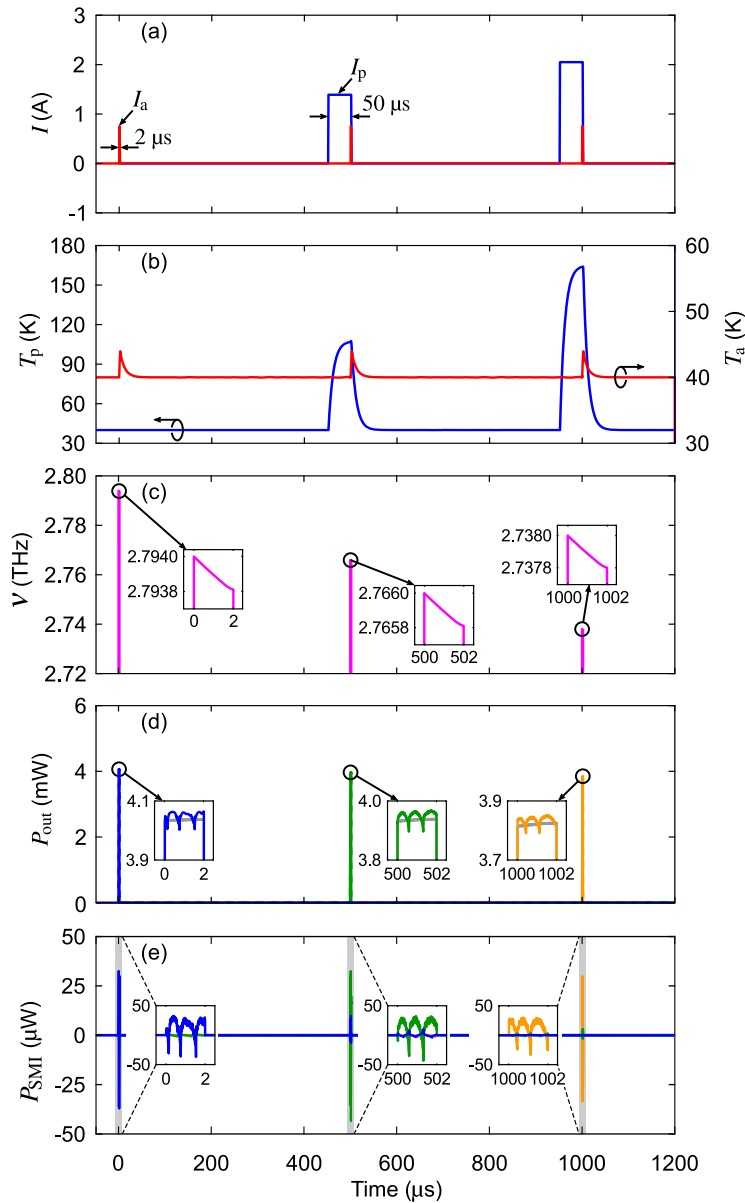


Fig. 3. Self-mixing response at three different frequency bands generated by LFI with thermal modulation in a coupled-cavity THz QCL: (a) the active cavity driving current I_a and passive cavity driving current I_p ; (b) the time varying lattice temperature in the passive and active cavity T_p and T_a ; (c) the emission frequency of active cavity of the CC THz QCL ν , where three continuous frequency red shifts are shown in three insets, respectively; (d) the output power of each emission mode P_{out} . The insets show the fine power features at the peak of each dominant mode, where blue, green, and orange solid curves indicate the output power of mode 4, 3, and 2 under optical feedback (target reflectivity $R = 0.7$) respectively. The grey lines in each insert denotes output power of the dominant mode without optical feedback; (e) the SM signal P_{SMI} , i.e. the difference between the blue, green, and orange and their respective grey traces in (d). The grey region in (e) denotes the time period illustrated in each inserts.

Based on the mode tuning results shown in Fig. 2, the passive cavity currents of 0 A, 1.39 A, and 2.05 A were chosen, to obtain the dominant modes M4, M3, and M2 respectively (2.794, 2.766, and 2.738 THz respectively) whilst maintaining the passive cavity in non-lasing conditions. The pulse durations for the passive cavity are all 50 μs in order to reach the steady state lattice temperature change ΔT_p , while the active cavity was driven by three pulses of amplitude 0.75 A and duration 2 μs , as shown in Fig. 3(a). The two drive currents applied to the coupled cavities are synchronized so that both pulses attain the OFF state simultaneously. This ensures that the narrow active cavity pulses are applied when the lattice temperature is steady in the passive cavity.

The passive cavity current is modulated with low duty cycle of 10 % in order to mitigate the effects of thermal cross-talk between the two cavities. The duration of the pulses, their respective duty cycles and the relative timings are adjusted so that the thermal crosstalk is not affecting the operation of the device. The cold finger temperature T_0 is fixed at 40 K in this work. The temporal evolution of the lattice temperature in the passive cavity and active cavity are shown in Fig. 3(b). The resulting mode hopping as well as continuous changes in the emission frequency at each mode are shown in Fig. 3(c). Continuous frequency tuning of 245 MHz is observed for each of the dominant modes (M4, M3, and M2), which is induced by the lattice temperature variation in the active cavity of 4.9 K (self-heating effect) when it is switched ON by the drive current.

Figure 3(d) shows the effects of optical feedback on the laser output power; variation in the output power is the source of the SM interferometric signal. The output power with optical feedback for M4, M3, and M2 are shown in Fig. 3(d) by blue, green, and orange lines, respectively. The output power without optical feedback is shown by grey solid lines for reference. The SM signals (the AC component of the power envelope with feedback), at three different THz frequencies spaced by 28 GHz are shown in Fig. 3(e) by blue, green, and orange lines, respectively, and are the difference between the blue, green, orange and their respective grey traces in Fig. 3(d).

The eigenmode frequencies and mode spacing frequency can be designed by means of the CC THz QCL parameters [45] in order to align with the target spectral features of interest. The results suggest that the SM signals at various frequency bands may be obtained simultaneously by using self-heating effects in both cavities, thereby enabling THz sensing or imaging over a wide spectral range so that unique spectral features of a target under test at multiple frequency ranges can be obtained simultaneously. Experimentally, the SM signal can be acquired not only from the power variations, but also from the more conveniently measured accompanying changes in the laser compliance voltage [65].

4. Conclusion

In conclusion, we established multi-mode RREs for a CC THz QCL subject to optical feedback, and thermal model for the coupled-cavities. We analyzed mode hopping and continuous frequency tuning in CC THz QCLs via self-heating induced by separate drive pulses applied to the passive and active cavities. We demonstrated in model the feasibility of LFI at various THz frequency bands using a single device. The results are of primary interest for the development of multi-spectral LFI sensing and imaging with pulse-driven tunable THz QCLs. The model proposed here forms a basis for future ultra-high-speed THz multispectral imaging systems and sensors for material identification and detection. In addition, the model presented in this work provides numerical platform for prediction and exploration of lasing and thermal dynamics in multi-mode QCLs under optical feedback.

Funding

Australian Research Council Discovery Project (DP160103910); Engineering and Physical Sciences Research Council (EPSRC), UK (COTS programme EP/J017671/1, and EP/J002356/1); European Cooperation in Science and Technology (COST) (BM1205 Action). X. Q. acknowledges support from the UQ Postdoctoral Research Fellowship programme; Y.L.L. acknowledges support from Queensland Government's Advance Queensland Program; E.H.L. and A.G.D. are grateful for support from the Royal Society and Wolfson Foundation.